Title

Simulation of experimental synthetic DNA tracer transport through the vadose zone

Authors

Wang, Chaozi
Liu, Geng
McNew, Coy P
et al.

Publication Date

2022-09-01

DOI

10.1016/j.watres.2022.119009

Peer reviewed

Simulation of experimental synthetic DNA tracer transport through the vadose zone

Chaozi Wang[a,b**], *Geng Liu*[a], *Coy P. McNew*[b], *Till Hannes Moritz Volkmann*[c], *Luke Pangle*[d], *Peter A. Troch*[c,e], *Steven Lyon*[f,g,h], *Minseok Kim*[c,i], *Zailin Huo*[a], *Helen E. Dahlke*[b,*]

[*] Corresponding author: Tel.: (530) 752-1130; E-mail: hdahlke@ucdavis.edu

[**] Co-corresponding author: Tel.: + 86 18510006639; E-mail: chaoziwang@cau.edu.cn

[a] College of Water Resources and Civil Engineering, China Agricultural University, Beijing 100083, China

[b] Department of Land, Air, and Water Resources, UC Davis, Davis, CA 95616, USA

[c] Biosphere2, University of Arizona, Oracle, AZ 85739, USA

[d] Department of Geosciences, Georgia State University, Atlanta, GA 30303, USA

[e] Department of Hydrology and Water Resources, University of Arizona, Tucson, AZ 85721, USA

[f] The Nature Conservancy Southern New Jersey Office, Delmont, NJ 08314, USA

[g] Department of Physical Geography, Stockholm University, Stockholm, Sweden

[h] School of Environment and Natural Resources, The Ohio State University, Columbus, OH, USA

[i] Department of Geography and Environmental Engineering, Johns Hopkins University, Baltimore, MD 21218, USA

Abstract

Although multiple experimental studies have proven the use of free synthetic DNA as tracers in hydrological systems, their quantitative fate and transport, especially through the vadose zone, is still not well understood. Here we simulate the water flow and breakthrough of deuterium (D) and one free synthetic DNA tracer from a 10-day experiment conducted in a transient variably saturated $1m^3$ 10-degree sloped lysimeter using the HYDRUS-2D software package. Recovery and breakthrough flux of D (97.78%) and the DNA tracer (1.05%) were captured well with the advection-dispersion equation (R^2 = 0.949, NSE = 0.937) and the Schijven and Šimůnek two-site kinetic sorption model recommended for virus transport modeling (R^2 = 0.824, NSE = 0.823), respectively. The degradation of the DNA tracer was very slow (estimated to be 10% in 10 days), because the "loamy sand" porous media in our lysimeter was freshly crushed basaltic tephra (i.e., crushed rocks) and the microbes and DNase that could potentially degrade DNA in regular soils were rare in our "loamy sand". The timing of the concentration peaks and the HYDRUS-2D simulated temporal and spatial distribution of DNA in the lysimeter both revealed the role of the solid-water-air contact lines in mobilizing and carrying DNA tracer under the experimental variably saturated transient flow condition. The free DNA was nearly non-selectively transported through the porous media, and showed a slightly early breakthrough, possibly due to a slight

effect of anion exclusion or size exclusion. Our results indicate that free DNA have the potential to trace vadose zone water flow and solute/contaminant transport, and to serve as surrogates to trace viral pathogen pollution in soil-water systems. To our knowledge, this study is the first to simulate transport mechanisms of free synthetic DNA tracers through real soil textured porous media under variably saturated transient flow condition.

Key words: synthetic DNA tracer, soil-water systems, variably saturated, HYDRUS-2D, vadose zone, viral pathogen pollution

1. Introduction

The use of synthetic DNA (deoxyribonucleic acid) to trace environmental flow and contaminant transport has become popular in recent years (Liao et al., 2018). This is in large part due to the nearly limitless number of unique nucleotide sequences available, as well as its high specificity, non-toxicity, and high detection sensitivity. The synthetic DNA used in most DNA tracer studies to date is produced by automated standard oligonucleotide synthesis (Sabir et al., 1999) and differs from naturally occurring DNA (single- or double-stranded) mainly in molecule length. Naturally occurring DNA strands are often several orders of magnitude longer (e.g., *Escherichia coli* DNA molecule: 4.7×10^6 base pairs) than the strands used in DNA tracer studies (mostly < 200 base-pairs or nucleotides). The synthetic DNA can be used either in its free form or can be encapsulated to form a tracer (Dahlke et al., 2015). To date the use of synthetic DNA as tracer

has mainly been in the form of “proof of concept” studies that focused on DNA tracer transport in comparison to conservative solutes such as Cl^-, Br^- or fluorescent dyes (Pang et al., 2020).

When free DNA is present in soil water, DNA molecules form colloidal particles that interact (e.g. attach, detach) with soil particles. Since synthetic DNA molecules are negatively charged when pH is above 5.0 (Xue and Feng, 2018), the degree of attachment of DNA molecules onto solid surfaces largely depends on the material type and the physico-chemical properties of the water the DNA is transported with (Ptak et al., 2004). DNA attachment to clay minerals has been shown to be several orders of magnitude higher than to sand grains (Lorenz and Wackernagel, 1987). Similar to other colloids, the attachment of DNA to soil particles is also directly influenced by pH, ionic strength and cation valence (Lorenz and Wackernagel, 1987; Wang et al., 2020). For example, increased attachment of DNA was observed with increasing presence of bivalent cations such as Ca^{2+} and Mg^{2+} than monovalent cations (e.g., Na^+) due to the cation bridge (Xue and Feng, 2018). Enzymatic degradation of DNA is enhanced in the presence of bacterial activity (Romanowski et al., 1993), but there is evidence that attachment onto minerals or colloids inhibits degradation (Pang et al., 2020). Further, the attachment of DNA molecules onto solid surfaces was found to be faster and temperature dependent compared to desorption (Lorenz and Wackernagel, 1987). Both the length of the DNA and the surface properties of the porous media influence the adsorption/desorption and recovery rate of DNA (Zhang et al., 2021). It has been found that the degradation of the synthetic DNA tracer was proportional to its length, and the degradation reaction follows quasi-first order kinetics (Mikutis et al., 2019). The presence of some divalent or multivalent cations, unsuitable pH, strong microbial activity,

elevated temperature and sunlight have all been found to accelerate the degradation rate of synthetic DNA tracer (Mikutis et al., 2019).

Most of the studies investigating DNA tracer transport through porous media were under saturated and steady-state conditions, e.g. Zhang et al. (2021). Application of DNA tracers in vadose zone systems, undergoing frequent wetting- and drying-cycles that create unsaturated or variably saturated conditions have been very rare to date. To our knowledge, Wang et al. (2019) were the first who study transport of encapsulated single-stranded DNA tracers in a transient flow (i.e., variably saturated) system. They found that in comparison to a conservative tracer (deuterium), the particulate DNA tracers (~850 nm diameter) traveled at a higher velocity and had a mass recovery rate highly dependent on the availability of preferential pathways, the timing of the tracer injection, the precipitation input and the water table dynamics within the lysimeter.

Among the studies published to date, a few studies have provided quantitative understanding of DNA tracer fate and transport through porous media, i.e., compared model simulation with experimental data. Sharma et al. (2012) used a simple 1D advection-dispersion model to capture the breakthrough of the polylactic acid (PLA)-microsphere-encapsulated DNA tracer transport through a saturated very coarse sand column. The advection-dispersion model seemed to suggest that the PLA-microsphere-encapsulated DNA tracer moved through saturated coarse sand column at the same speed as water. Similarly, Aquilanti et al. (2013) used a simple 1D advection-dispersion model to capture the breakthrough of free DNA tracer transport through a column consisted of aquifer material analyte. It was found that the breakthrough of the free DNA tracer was earlier and less dispersed than that of the conservative tracer, KCl. Mikutis et al.

(2018) used a 1D advection-dispersion transport equation to capture the breakthrough of the silica encapsulated DNA tracer and a solute tracer, uranine, transport through sand column (particle size range 0.20–0.63 mm). It was found that the breakthrough of the silica encapsulated DNA tracer was faster than the solute tracer, and the larger the tracer size the faster its breakthrough, indicating that the particulate tracers only access larger pores or fractures. Pang et al. (2014) used the colloid filtration theory adopted for pulse injection and a 1D two-site kinetic model, both implemented in HYDRUS-1D, to capture the breakthrough of DNA-labeled protein-coated silica nanoparticles transport through beach sand columns. The two kinetic attachment sites were assumed to be one reversable attachment site and one irreversible attachment site. It was found that the DNA-labeled protein-coated silica nanoparticles could better represent the reduction of the target viruses, rotavirus and adenovirus, than the traditional virus surrogate, MS2 phage. Clemens et al. (2020) used a 1D advection dispersion equilibrium model and incorporated a first-order reduction term to capture the breakthrough of DNA-labelled-glycoprotein-coated silica nanoparticles (DGSnp) transport through intact soil cores. It was found that the DGSnp could better represent the reduction of the target virus, rotavirus, than the traditional virus surrogate, MS2 phage. However, all these simulations of the transport of DNA traces were conducted under saturated and steady-state conditions.

Understanding the transport of DNA tracer in porous media under variably saturated transient flow conditions is crucial in exploring its application to soil or the vadose zone where flow conditions vary constantly. Falling in the size range of colloid (1nm-10μm), DNA tracer behave like colloids when transported through the vadose zone. Thus, under saturated condition, the retention and remobilization of DNA tracer is dominated by straining, and attachment

to/detachment from solid–water interfaces (SWIs). However, under variably saturated transient flow conditions, a lot more complexity emerges, such as attachment to/detachment from air–water interfaces (AWI), air–water–solid (AWS) contact lines scouring, film straining, and entrapment in/release from immobile water zones (Wang et al., 2020). Due to all these challenges, to the best of our knowledge, no study has validated the transport of free synthetic DNA tracers through the vadose zone (i.e. transient flow system characterized by wetting-drying cycles) using a flow and colloid transport model.

Therefore, the objective of our study is to provide experimentally validated quantitative understanding of the fate and transport of a free synthetic DNA tracer through the vadose zone of a 1 m^3 sloped lysimeter under variably saturated transient flow condition. The breakthrough curve and the spatial and temporal distribution of the free synthetic DNA tracer was simulated using the HYDRUS-2D software package and the two-site kinetic sorption model from Schijven and Šimůnek (2002).

2. Materials and methods

2.1 The free DNA tracer and its quantification

The T12 DNA sequence was designed by, first, generating a random 200-nucleotide sequence using the freely available GeneDesign Random DNA generator (http://54.235.254.95/cgi-bin/gd/gdRandDNA.cgi, last accessed September 22, 2020). Next, the DNA sequence was tested with the National Center for Biotechnology Information's (NCBI) Nucleotide Primer-BLAST Tool (http://www.ncbi.nlm.nih.gov/tools/primer-blast/, last accessed September 22, 2020) to identify

any potential overlap with known genomes. We used the IDT DNA PrimerQuest Tool (https://www.idtdna.com/site/account/login?returnurl=/calc/analyzer) to determine an 88-nucleotide subsequence within the 200-nucleotide for which primers had annealing temperatures between 55 and 60 °C. The annealing temperature resulting in the highest efficiency for the T12 DNA sequence was determined by conducting a thermal gradient experiment for optimizing annealing temperature on the Bio-Rad CFX96 Touch. The best annealing temperature for the T12 tracer was 55.7 °C.

Table 1. The sequence of the synthetic DNA tracer.

	DNA sequence
T12	5'- C**CG TAG AGA TCT CCC ATC TGT CCT TTG** CTG AAG GTT AAA ACC CCG GAC CGC CTA GAA TAT TC*T TTC TTT AGC TCC AAA ATG GCC TCT* C -3'

Bold and underlined: forward primer
Italic and underlined: reverse primer

The concentration of the free DNA (T12 sequence, see Table 1) in the samples was estimated using quantitative real-time polymerase chain reaction (qPCR). qPCR samples were prepared for a 96-well plate by mixing 4 µl of each collected sample, with 5 µl of the SsoAdvanced™ Universal SYBR® Green Supermix, 0.4 µL of each forward and reverse primer, and 0.2 µL of nuclease-free water prior to analysis with a Bio-Rad CFX96 Touch (Hercules, CA, USA). Three replicates of each sample as well as 3 blanks and 7 standard triplicates (i.e., samples of known concentration ranging from 100 – 10^8 copies) were included on each plate and a standard curve was produced to relate the quantification cycle (C_q) value to DNA copy count. Standards were prepared with the native water used in the experiment to accommodate potential inhibition. DNA copy count for each sample was the mean of the three replicates calculated with the Bio-Rad

software (Bio-Rad CFX Manager 3.1) using the regression determination mode with baseline subtracted curve fit. If the standard deviation was more than 10% of the mean, another three replicates were run until the standard deviation was no more than 10% of the mean. The upper and lower DNA detection limits were defined by the portion of the standard curve where the C_q and DNA copy count correlate with an $R^2 \geq 0.99$ and the slope of the standard curve was used to estimate the efficiency which was between 85% and 100%. The detection range falls between 100 and 10^8 copies per sample, or 25 to 2.5×10^7 copies/µL, i.e., a sample with free DNA concentration less than 25 copies/ µL was tested to be negative on each plate. In this manner, the DNA copy count was always interpolated from standards included on each plate and never extrapolated. DNA copy counts were estimated based on a sample volume of 4 µL and then scaled to the observed discharge rate.

2.2 A brief summary of the experiment

The study presented here uses hydrological observations and deuterium and free DNA transport data from a 10-day controlled experiment conducted at the Landscape Evolution Observatory (LEO) within the Biosphere 2 (Oracle, AZ, USA; see Pangle et al. (2015)). The experiment use a sloped lysimeter, a miniature LEO (the miniLEO), with an inner length of 200 cm, inner width of 50 cm, inner depth of 100 cm, and a bed slope of 10 degrees (Figure S1). A 10-cm thick gravel layer (0.05 m^3) of late Pleistocene basaltic tephra with a grain size of ~1 cm was placed along the downslope face of the lysimeter, and then the upslope 190 cm of the lysimeter was packed with crushed late Pleistocene basaltic tephra (i.e. crushed rocks) with a grain size of loamy sand (3.2 % clay [< 2 µm]; 12.2 % silt [2-50 µm]; 84.6 % sand [50-2000 µm](Wang et al., 2019)), with rare microbes and organic matters compared to regular soil (Sengupta et al., 2016). The lysimeter

was equipped with a suite of hydrologic sensors consisting of a tipping bucket gauge (Onset RG3) at the outlet of the soil lysimeter to measure discharge and 15 water potential sensors (MPS-2, Decagon), 15 volumetric water content and temperature sensors (5TM, Decagon), 15 soil pore water samplers (Prenart Super Quartz sampler) were installed at three slope positions (downslope, midslope and upslope) and five depths (5, 20, 35, 50 and 85 cm), and 3 water level sensors (downslope, midslope and upslope; Campbell Scientific CS451) (Wang et al., 2019). In addition, the weight of the soil box was measured to estimate changes in storage. Data was recorded at 1-minute intervals.

A 10-day periodic transient flow and transport experiment was started on June 14, 2016, 35 days after the lysimeter was packed and 5 days after rainwater was applied periodically to prime the system. For the initiation and duration of the experiment, three rainfall pulses of 2-hr duration with a rainfall intensity of 30 mm hr^{-1} were applied each day: the first pulse was applied from 8:00 to 10:00, the second pulse from 12:00 to 14:00, and the third pulse from 16:00 to 18:00. The periodic transient regime was adopted to study the transport of water and two types of DNA tracers in a variably saturated system, which most closely resembles the wetting and drying cycles that occur in natural vadose zone systems. The 10-degree slope, the pre-packing and the periodic rainfall caused some of the loamy sand to enter the bottom part of the gravel, which was witnessed when excavating the lysimeter after the experiment. This fact was considered in the simulation model, and was described in details in the first paragraph of “S4. Inverse modeling details” in the Supporting Information.

During the experiment one conservative tracer (deuterium, D) and one free DNA tracer (i.e. unencapsulated, synthetic DNA) were applied to the lysimeter. The D was applied during all

three rainfall pulses on the first day of the experiment, while the free DNA tracer was applied on the second day of the experiment. During the experiment, four DNA-labeled particle tracers (synthetic DNA encapsulated in polylactic acid [PLA] polymer microspheres), each with their own unique DNA sequence, were also applied on the lysimeter as analyzed in Wang et al. (2019). In this study, we focus on the D and unpublished free DNA transport data from this transient flow experiment to provide experimentally validated quantitative understanding of the fate and transport of a free synthetic DNA tracer through vadose zone systems.

The D abundance in the tracer solution (i.e., applied rainfall) was 765‰ (equivalent to 2.8810×10^{-2} mmol/ml of semi-heavy water molecules (H^2HO)), while the D abundance in the other rainfall events and in the background soil water was -57‰ (equivalent to 1.5395×10^{-2} mmol/ml H^2HO). The D concentration in discharge was measured in real time at 1-minute intervals, relative to the Vienna Standard Mean Ocean Water with a Los Gatos Research DLT-100 Laser (Wang et al., 2019), and then converted to mmol/ml H^2HO for easier modeling. The details of the real time sampling and sample analysis were provided by Wang et al. (2019).

The synthetic free DNA tracer was applied on the second experimental day as a slug injection by pouring a 50 ml solution with a concentration of 2.64×10^{13} copies/ml along a 1 cm wide line across the soil surface (about 115-116 cm upslope from the seepage face) (Figure S1a). The injection took about 10 seconds to complete (Jun 25 13:00:00 to 13:00:10). The synthetic, HPLC-purified single-stranded DNA used in the experiment consisted of 88 nucleotides (see Table 1) and was purchased from Integrated DNA Technologies (IDT Inc., Coralville, Iowa, USA). Prior to application, the synthetic DNA was stored in 50 ml of 50 × molecular biology grade Tris–EDTA (TE) buffer (75834) (Fisher Scientific TE buffer) (when diluted to 1 × has a

pH of 8.0 and consisted of 10 mM Tris and 1 mM EDTA) to keep DNA negatively charged and well suspended and protected from degradation. Each DNA molecule is typically curled up into a rod with an estimated diameter and length of 2.4 nm and 29.4 nm, respectively (calculated according to Mandelkern et al. (1981)). The free DNA molecule therefore falls in the lower size range of colloids (1 nm ~ 10 μm) and is in many ways comparable to the size of known nanoparticles such as silver, gold or silica nanoparticles. However, the mass (26,857.4 Da) and structure of the single-stranded DNA molecule are more like biocolloids such as viruses and bacteriophages, which often consist of a single-stranded or double-stranded DNA or RNA wrapped by protein (Chu et al., 2001; Jin and Flury, 2002; Jin et al., 1997).

A 1 mL sample was taken from the free DNA tracer solution right before application to the lysimeter to determine the initial tracer mass. Discharge samples were collected in the trough at the bottom of the downslope face of the lysimeter (see Figure S1 and section "S1. Experiment details" in the Supporting Information for more information). Discharge was collected in sterilized 5 ml tubes (Eppendorf AG, Hamburg, Germany) every half hour during the first three days and every hour for the remainder of the experiment using a temperature controlled auto-sampler. The discharge samples were stored in a -20°C freezer until free DNA quantification by the qPCR method described above, which was finished within two weeks after the experiment. The discharged free DNA flux was determined by the product of concentration and discharge. And the recovery rate of free DNA was the ratio of discharged free DNA to total injection (50 ml solution with a concentration of 2.64×10^{13} copies/ml).

2.3 Water flow and deuterium tracer transport modeling

Because previous experiments proved that variation of soil properties, i.e. flow and transport pathways, along the width axis of the soil lysimeter was negligible (Sengupta et al., 2016; Wang et al., 2019), we chose to only consider the flow and transport along the length and depth (2D) axes of the sloped lysimeter. The 2D water flow in our variably saturated system can be described using a modified form of the Richards' equation (Šimůnek et al., 2008) (see section "S2. Water flow modeling" in the Supporting Information for details). And the D transport during transient water flow in the variably saturated system was simulated using an advection-dispersion equation (see section "S3. Deuterium tracer transport modeling" in the Supporting Information for details).

2.4 DNA tracer transport modeling

As mentioned in section 2.1, the mass and structure of the free DNA tracer is comparable to viruses and bacteriophages (Attinti et al., 2010; Chu et al., 2003; Jin et al., 2000). Hassanizadeh and Schijven (2000) showed that the breakthrough curves of bacteriophages (MS2 and PRD1) in column experiments could be described with a advection–dispersion model that incorporates attachment to two types of kinetic sites. The model assumes that the sorption sites on the solid phase can be divided into two fractions with different properties and various attachment and detachment rate coefficients. Schijven and Šimůnek (2002) were among the first to adopt and modify the two-site kinetic sorption model for transient flow system in HYDRUS. Although several numerical modeling codes are available for the simulation of colloid transport in transient

flow systems, the two-site kinetic sorption model developed by Schijven and Šimůnek (2002) for HYDRUS-2D (Šimůnek et al., 2008) described two different kinetic sorption sites simulated virus transport through soil better than other models. Therefore, we chose to adopt the two-site kinetic sorption model by Schijven and Šimůnek (2002) to simulate the transport of the DNA tracer in the miniLEO lysimeter:

$$\frac{\partial \theta C}{\partial t}+\rho_b \frac{\partial S_1}{\partial t}+\rho_b \frac{\partial S_2}{\partial t}=\frac{\partial}{\partial x_i}\left(\theta D_{ij}^{w}\frac{\partial C}{\partial x_j}\right)-\frac{\partial q_i C}{\partial x_i}-\mu_w \theta C-\mu_s \rho_b (S_1+S_2) \quad (1)$$

$$\rho_b \frac{\partial S_1}{\partial t}=\theta k_{a1} C-k_{d1}\rho_b S_1-\mu_s \rho_b S_1 \quad (2)$$

$$\rho_b \frac{\partial S_2}{\partial t}=\theta k_{a2} C-k_{d2}\rho_b S_2-\mu_s \rho_b S_2 \quad (3)$$

$$\theta D_{ij}^{w}=\lambda_L |q| \delta_{ij}+(\lambda_L-\lambda_T)\frac{q_i q_j}{|q|}+\theta D_w \tau \delta_{ij} \quad (4)$$

where C is DNA concentration in the aqueous phase (copies/ml), S is the concentration on kinetic sorption sites (copies/g), θ is the volumetric water content, ρ_b is the try bulk density (g/cm^3), x_i and x_j ($i=1,2$; $j=1,2$) are the spatial coordinates (cm) ($x_1=x$ is the horizontal coordinate and $x_2=z$ is the vertical coordinate (positive upward)), t is time (min), q_i is the *i-th* component of the volumetric flux density (cm/min), D_{ij}^{w} is the dispersion coefficient tensor (cm^2/min) for the liquid phase defined in Eq. 4 (Bear, 1972), μ_w and μ_s are the first-order degradation rate constants of the free and attached DNA tracers, respectively, D_w is the molecular diffusion coefficient in free water (cm^2/min), τ is a tortuosity factor, $|q|$ is the absolute value of the Darcy's fluid flux density (cm/min), δ_{ij} is the Kronecker delta function, and λ_L and λ_T are the longitudinal and transverse dispersion coefficients (cm), respectively, k_a and k_d are the first-order attachment and

298 detachment rate coefficients, respectively (min^{-1}), and subscripts 1 and 2 refer to the two different
299 kinetic sites, respectively.

300

301 *2.5 Inverse modeling*

302 The above physically-based equations were numerically solved for the miniLEO lysimeter using
303 the HYDRUS-2D, a main-stream software package solving water flow and solute/contaminant
304 transport problems in the vadose zone (Šimůnek et al., 2013; Šimůnek et al., 1998; Šimůnek et
305 al., 2008; Šimůnek et al., 2016). Firstly, water flow was simulated by inversely solving the soil
306 hydraulic properties (residual water content, the inverse of the air-entry value, pore-size
307 distribution index, and saturated hydraulic conductivity) of the loamy sand by fitting to the
308 measured discharge, the measured pressure head (i.e. water table) at upslope, midslope and
309 downslope locations (Figure S2b, Observation Nodes 3, 2, 1, respectively), and volumetric soil
310 content at three locations (Figure S2b, Observation Nodes 4, 5, 6, respectively). Secondly, in
311 order to keep the widely accepted relationship that the longitudinal dispersivity (λ_L) is 5-10 times
312 larger than the transverse dispersivity (λ_T) (Abbasi et al., 2003), based on the well captured water
313 flow, the D flux was simulated via inversely solving the longitudinal and transverse dispersivities
314 by fitting to the measured D flux via trial and error. Each trialed pair of λ_L and λ_T met the
315 relationship that λ_L is 5-10 times larger than λ_T. Finally, to guarantee the solution uniqueness of
316 the DNA transport model, based on the well captured water flow and inherited the longitudinal
317 and transverse dispersivities obtained by the D flux, the DNA flux was simulated via 1)
318 estimating the degradation rates of the free and attached DNA tracers by trial and error, 2)
319 inversely solving the attachment and detachment rates of the two kinetic sorption sites of the

loamy sand by fitting to the measured DNA flux, and 3) assigning the best fit attachment and detachment rates obtained for loamy sand to the corresponding parameters of gravel. Then, a simple local sensitivity analysis was conducted to see if the obtained parameters are the best fit and if the model is insensitive to some of the parameters. The domain setup and initial and boundary conditions as well as details of the model calibration and validation are described in Supporting Information "S4. Inverse modeling details" and "S6. Sensitivity analysis"..

3. Results and Discussion

3.1 Water flow

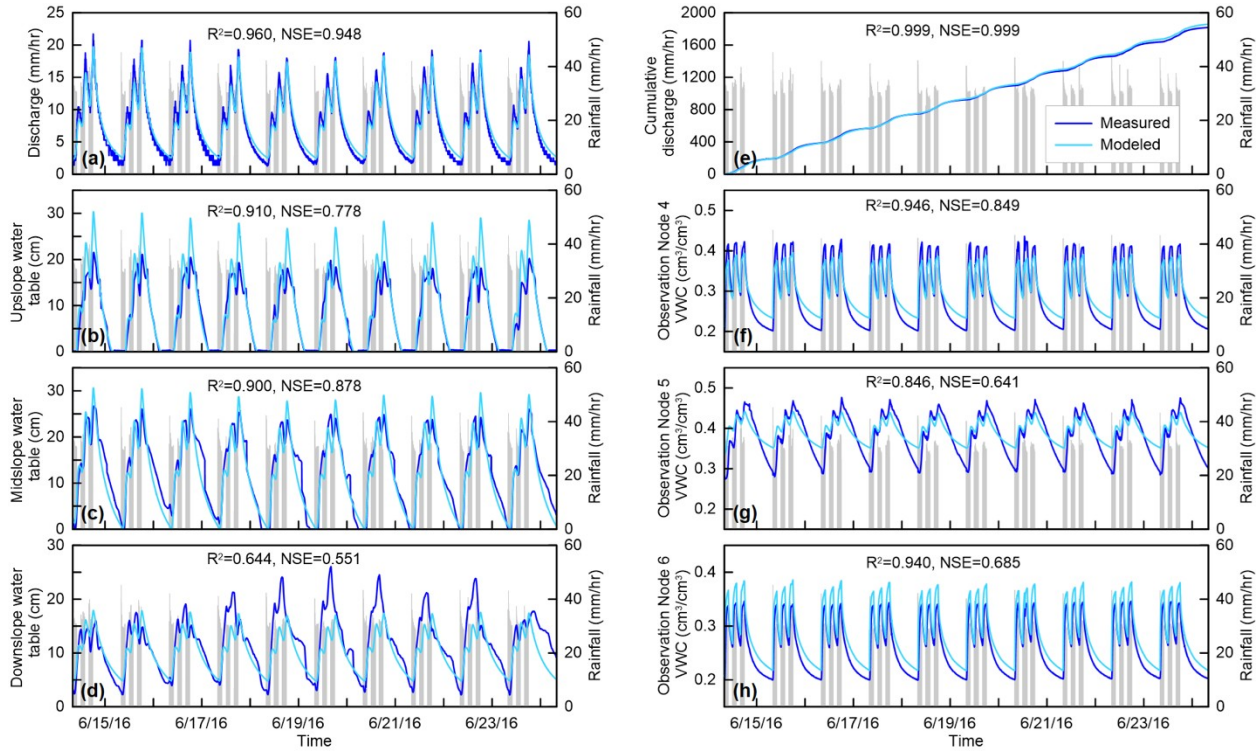

Figure 1. Comparison of the measured and modeled discharge (a), cumulative discharge (e), water table at three slope positions (upslope (b), midslope (c) and downslope (d)), and volumetric water content at three locations (Observation Node 4 (f), Observation Node 5 (g) and Observation Node 6 (h)). The grey bars indicate the rainfall condition for each plot.

Table 2. HYDRUS inversely solved best fit soil hydraulic parameters, and D and DNA transport parameters.

		θ_r [b]	θ_s [a]	α (1/cm) [b]	n [b]	K_s (cm/min) [b]	l [a]	ρ_b (g/cm^3) [a]
Water flow	Loamy sand	2.63×10^{-3}	0.469	0.0191	2.20	0.294	0.5	1.48
	Gravel	2.19×10^{-5}	0.333	0.145	2.68	30	0.5	1.73
		λ_L (cm) [c]	λ_T (cm) [c]	D_d (cm^2/min) [a]				
D	Loamy sand	0.15	0.03	1.33×10^{-3}				
	Gravel	0.01	0.002	1.33×10^{-3}				
		λ_L (cm) [d]	λ_T (cm) [d]	D_d (cm^2/min) [a]	μ_w (1/min) [e]	μ_s (1/min) [e]		
DNA	Loamy sand	0.15	0.03	2.70×10^{-5}	7.32×10^{-6}	7.32×10^{-7}		
	Gravel	0.01	0.002	2.70×10^{-5}	7.32×10^{-6}	7.32×10^{-7}		
		k_{a1} (1/min)[f]	k_{d1} (1/min)[f]	k_{a2} (1/min)[f]	k_{d2} (1/min)[f]			
DNA	Loamy sand	1.58×10^{-3}	1.24×10^{-3}	1.96×10^{-3}	5.72×10^{-6}			
	Gravel	1.58×10^{-3}	1.24×10^{-3}	1.96×10^{-3}	5.72×10^{-6}			

θ_r and θ_s are the residual and saturated volumetric water contents, α is the inverse of the air-entry value, n is the pore-size distribution index, K_s is the saturated hydraulic conductivity, l is the pore-connectivity parameter, ρ_b is the bulk density. λ_L and λ_T are the longitudinal and transverse dispersivities, D_d is the molecular diffusion coefficient, μ_w and μ_s are the first-order degradation rate constants of the free and attached DNA tracers, respectively, k_a and k_d are attachment and detachment rate coefficients, respectively, and subscripts 1 and 2 referring to the two different kinetic sites.

[a] *Prescribed parameters.*

[b] *Inversely solved parameters.*

[c] *Parameters inversely solved by trial-and-error.*

[d] *DNA transport parameters inherited from D transport parameters.*

[e] *Parameters estimated by trial-and-error.*

[f] *Parameters inversely solved for loamy sand and assigned to gravel.*

Table 3. Mass balance of water, D and DNA.

Water		D		DNA	
Total Rainfall (mm)	1,759	Total Injection (mmol)	2,443	Total Injection ($\times 10^{13}$ copies)	132
Total Evaporation (mm)	36	Total Discharged (mmol)	2,433	Total Discharged ($\times 10^{13}$ copies)	1.42
Total Discharge (mm)	1,721	Total Retention (mmol)	10	Total Retention ($\times 10^{13}$ copies)	117.38
Change of Storage (mm)	2			Total Degradation ($\times 10^{13}$ copies)	13.2

The mass balance data for water and D is from Wang et al. (2019)

The discharge (R^2 = 0.961 and Nash-Sutcliffe Efficiency (NSE) = 0.948) and cumulative discharge (R^2 = 0.999 and NSE = 0.999) from the miniLEO lysimeter (Figures 1a and 1e) were captured very well by the Richards' equation. Because of the high precipitation input in the system (180 mm/day) evaporation losses from the lysimeter were omitted in the HYDRUS simulation (Table 3). The goodness of fit measures decreased for the simulated water table at the midslope (R^2 = 0.900 and NSE = 0.878, Figure 1c), upslope (R^2 = 0.909 and NSE = 0.778, Figure 1b), and downslope position (R^2 = 0.644 and NSE=0.551, Figure 1d). And the goodness of fit measures were satisfactory for the simulated volumetric water content at the Observation Node 4 (R^2 = 0.946 and NSE=0.849, Figure 1f), 5 (R^2 = 0.845 and NSE=0.641, Figure 1g) and 6 (R^2 = 0.940 and NSE=0.685, Figure 1h). The small discrepancies between the observed and the simulated water tables and volumetric water contents over the duration of the experiment might be attributed to the gradual settling of the porous media in the experimental lysimeter, making

the porous media not static. In addition, air entrapment and hysteresis effects of the cyclical rainfall events could also have caused some discrepancies in the discharge behavior. Overall, the satisfactory simulation of discharge, water table and volumetric water content dynamics suggests that the simulated water flow field in the system was very similar to the experimental observation, which provided a solid foundation for the simulation of the D and DNA transport in the system.

3.2 Transport of D tracer

The D tracer concentration started to rise during the third rainfall event on Day 1 of the experiment and peaked at the end of the third rainfall event on Day 2 (Figure 2b). This indicated that the D tracer applied during the first rainfall event on Day 1 started to reach the outlet during the third rainfall event on the same day, and that the regular rainwater applied on Day 2 started to dilute the D in the discharge at the end of the third rainfall event on Day 2.

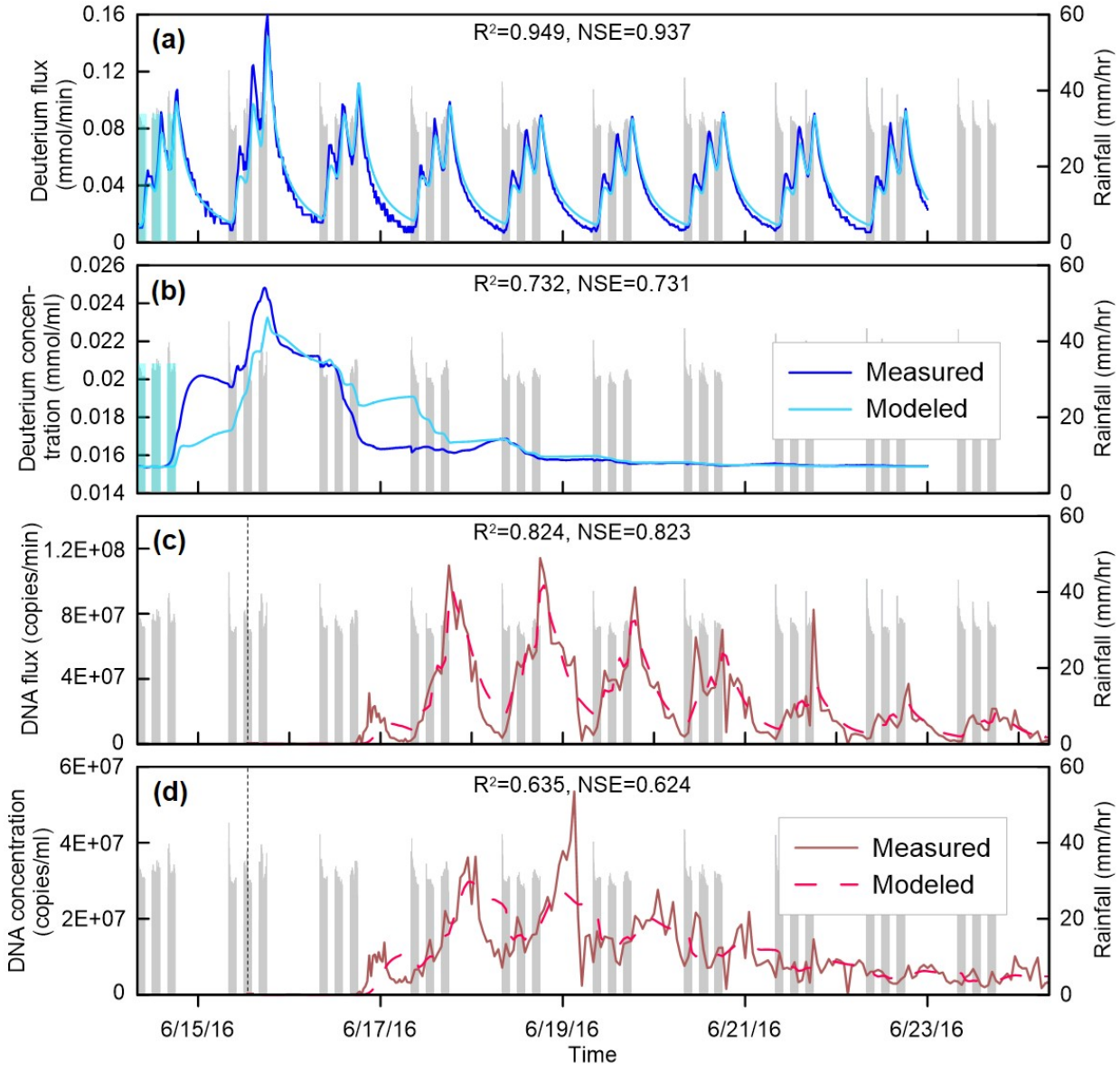

382

383 **Figure 2.** Deuterium flux (a) and concentration (b, breakthrough curve, i.e., transit time
384 distribution), and DNA flux (c) and concentration (d, breakthrough curve, i.e., transit time
385 distribution). The grey bars indicate the rainfall condition for each plot. Light blue bars in (a) and
386 (b) show the injection of the Deuterium tracer. The black dotted lines in (c) and (d) indicate the
387 input of DNA tracer solution.

388

One potential difficulty when simulating D transport is the occurrence of isotopic fractionation due to evaporation (Leibundgut et al., 2011). Hence, D behaves differently compared to conservative solutes that remain in the system when water evaporates (Stumpp et al., 2012). However, when simulating the water flow of the miniLEO experiment, we assumed that evaporation was negligible in the system. The mass balance of water (Table 3) and the accurate simulation of cumulative discharge (Figure 1e) confirmed this assumption. Therefore, we could treat D as a conservative solute in our simulation.

The D flux was simulated by adopting the best fit soil hydraulic parameters and using a mutual heavy water diffusion coefficient of D in water from the literature (Dahal and Adhikari, 2012; Meng et al., 2018) (D_d =1.33 × 10^{-3} cm^2/min) and inversely solve the longitudinal and transverse dispersivities. Under variably saturated conditions, the dispersivities depended not only on the dimensions of the lysimeter, the median diameter of the porous media particle, free-water diffusion coefficient of the solute, the pore flow velocity (Carey et al., 2018; Chrysikopoulos and Katzourakis, 2015; Cupola et al., 2015; Mahmoodlu et al., 2020), but also on the water content in the unsaturated soil (Mortensen et al., 2006; Raoof and Hassanizadeh, 2013). The trial-and-error obtained best fit values were λ_L = 0.15 cm and λ_T = 0.03 cm for the loamy sand and λ_L = 0.01 cm and λ_T = 0.002 cm for the gravel (Table 2). The D flux and concentration were well captured by the advection-dispersion equation (Bear, 1972; Schijven and Šimůnek, 2002) (R^2 = 0.949 and NSE = 0.937 for flux, R^2 = 0.732 and NSE = 0.731 for concentration, Figures 2a and 2b). Sensitivity analysis results showed that a small change (5%) of any one of these four dispersivities would lead to the decrease of the NSE of the simulated D concentration (Figure S5). Therefore, the obtained combination was accepted as the best fit dispersivities. However, the

411 concentration peak was underestimated, and the predicted concentration decreased slower than
412 the measured one (Figure 2b). We expect that this might be due to some errors in the real-time
413 sampling and measurement of D, as well as the gradually changing experimental porous media,
414 not represented by the static porous media used in the simulation.

415 *3.3 Transport of free DNA tracer*
416

417 The DNA tracer concentration started to rise at the end of the third rainfall event on Day 3 and
418 exhibited clear successive peaks every day for the remainder of the experiment (Figure 2d).
419 DNA concentration peaked every day during the night, when there was no rainfall input (Figure
420 2d), when the system was draining, and discharge was low (Figure 1a). This appearance of DNA
421 tracer concentration peaks opposite to the discharge peaks is consistent with findings by
422 Powelson and Mills (2001), who observed effluent colloid concentration peaks that were out of
423 phase with the discharge and water content peaks in a variably saturated flow system. Crist et al.
424 (2004) demonstrated that under partly saturated condition (like our experiment) negatively
425 charged hydrophilic colloids (i.e., our free DNA under the pH of 8.45 ± 0.60, the electrical
426 conductivity of 271.7 ± 63.2 μS/cm, and the ionic strength of 3.53 ± 0.82 mmol/L, at which the
427 free DNA suspension is very stable) were trapped by and moved with air-water-solid (AWS)
428 contact lines. According to Wang et al. (2020), the movement of the drying front AWS contact
429 lines could mobilize DNA attached to SWIs; whereas the movement of the wetting front AWS
430 contact lines could attach DNA to SWIs. Under our experimental condition, the movement of
431 drying front AWS contact lines was initiated by ceasing of rainfall. And the longest continuous
432 movement of the drying front AWS contact lines mobilizing and carrying DNA was after the

ceasing of the last rainfall on each day, i.e. during the night. This explains why our DNA concentration peaks were during the night.

Total recovery of free DNA at the end of the 10-day experiment was 1.08% (Table 3, 1.42×10^{13} copies by observation and 1.46×10^{13} copies by modeling) and, as indicated in Figure 2d, the breakthrough of the free DNA did not stop before the end of the experiment was reached, indicating that if the experiment would have been conducted for several more days, the recovery rate could have been higher, though still far from the recovery rate of the D tracer (97.78%, Table 3). To eliminate the time limit of the experiment and find the total recovery rate of free DNA, the model was run for 50 days, and the recovery rate was 1.20 % (1.59×10^{13} copies by modeling, Figure S7). The low recovery rate of DNA was mainly due to the irreversible attachment of the free DNA at solid-water interfaces, i.e., the surface of the soil particles, which will be discussed below. Our recovery rate of the free DNA tracer was comparable to the double-stranded free DNA tracers of high recovery tested by Pang et al. (2020), and one order of magnitude higher than their double-stranded free DNA tracers of low recovery (Figure 8b of Pang et al. (2020)).

The simulation of the DNA flux and concentration with the two-site kinetic sorption model (R^2 = 0.824 and NSE = 0.823 for flux, R^2 = 0.635 and NSE = 0.624 for concentration, Figures 2c and 2d) was reasonably good. The diffusion coefficient of the 88 nucleotides single-stranded DNA molecule was adopted from literature (Nkodo et al., 2001) (D_d = 2.70×10^{-5} cm^2/min). The longitudinal and transverse dispersivities were inherited from the best fit values of the D transport: λ_L = 0.15 cm and λ_T = 0.03 cm for loamy sand, and λ_L = 0.001 cm and λ_T = 0.002 cm for gravel (Table 2). The first-order degradation rate constants of the free DNA tracer (μ_w) and

attached DNA tracer (μ_s) were found to be 7.32×10^{-6} min^{-1} and 7.32×10^{-7} min^{-1}, respectively, by trial and error. The 7.32×10^{-6} min^{-1} first-order degradation rate constant was equivalent to a degradation of only 10% free DNA tracers in the 10-day experiment, which was much lower than the free DNA degradation rate in other soils (Sirois and Buckley, 2019). It was reasonable considering that the "loamy sand" porous media in the miniLEO was freshly crushed basaltic tephra (i.e., crushed rocks) and the microbes and DNase that could potentially degrade DNA in regular soils were rare in the miniLEO soil (Sengupta et al., 2016). A previous experiment showed that after the freshly crushed "loamy sand" basaltic tephra was irrigated for 18 months, there emerged some microbes (Sengupta et al., 2016); whereas, our experiment only lasted for only 10 days. The 7.32×10^{-7} min^{-1} first-order degradation rate constant of attached DNA was one order of magnitude less than that of free DNA, which was consistent with previous findings that attachment of free DNA onto minerals or colloids inhibits its degradation (Pang et al., 2020). The sensitivity analysis showed that the model was insensitive to μ_s as long as it was much less than μ_w (Figure S6a and S6c), which means that the attachment to porous media could indeed largely inhibit the degradation of DNA.

The initial values of the attachment and detachment rates for both sites of the two-site kinetic sorption model were set as $k_{a1} = k_{d1} = k_{a2} = k_{d2} = 1.0 \times 10^{-4}$ min^{-1} according to the adsorption rate constant measured for a 90 bp double-stranded DNA transport through a sand column by (Zhang et al., 2021). Since it was found that the water flow, and, therefore, the DNA transport rarely pass the gravel layer (Figure S4), only the four attachment and detachment rates of the loamy sand were inversely solved, to avoid simultaneously fitting too many parameters and to guarantee the uniqueness of the solution. And then it was assumed that the four attachment and detachment

rates of the gravel were the same as those of the loamy sand. This assumption was supported by the sensitivity analysis showing that the model is sensitive to the four attachment and detachment rates of the loamy sand (except for k_{d2}), but insensitive to the four attachment and detachment rates of the gravel (Figures S6b and S6d). For the kinetic sorption site 1, the best fit detachment rates were close to the attachment rates (Table 2, $k_{d1} = 1.24 \times 10^{-3}$ min^{-1} and $k_{a1} = 1.58 \times 10^{-3}$ min^{-1} for both loamy sand and gravel), which suggests that the attachment of DNA molecules to this site was reversible. In contrast, for the kinetic sorption site 2, the best fit detachment rates were three orders of magnitude less than the attachment rates (Table 2, $k_{d2} = 5.72 \times 10^{-6}$ min^{-1} << $k_{a2} = 1.96 \times 10^{-3}$ min^{-1} for both loamy sand and gravel), which suggests that for kinetic sorption site 2 the attachment process was almost irreversible. And sensitivity analysis showed that model worked well as long as k_{d2} was much less than k_{a2} (Figures S6b and S6d).

The overall fitness of the 2D two-site kinetic sorption model to the free synthetic DNA breakthrough was reasonably good (Figure 2d). The overall trends were very similar, but the estimated concentration was smoother than the measured concentration, i.e. the peaks were underestimated, and the valleys were overestimated (Figure 2d). Similar to the findings of Schijven and Šimůnek (2002), the two-site kinetic sorption model does an excellent job in capturing the gradual decrease in DNA tracer concentrations over the course of the experiment. However, as can be seen from Figure 2d, the two-site kinetic sorption model does not completely describe the peaks of the measured DNA tracer breakthrough curves, indicating that other types of kinetic sites might have been present in the system influencing the attachment/detachment of DNA molecules or that DNA transport is additionally complicated by effects of soil heterogeneity or dimensionality of the problem. Also, the way the DNA concentration was

499 measured caused the data to scatter. A 4μl subsample was taken from each discharge sample for
500 DNA copy analysis and then the concentration (e.g. measured copies/ml) was multiplied by 250
501 to estimate a total concentration for the sample. This means that a small error in mixing the
502 sample and taking the subsample for qPCR analysis would be amplified by a factor of 250 in the
503 measured DNA concentration. Finally, the first three simulated peaks were slightly later than the
504 measured ones, which could be attributed to the negatively charged DNA and the like-charged
505 soil particles, or the colloidal-sized DNA tracer, possibly leading to a slight anion exclusion or
506 size exclusion effect, resulting in slightly earlier breakthrough than simulated.

507 Validated by DNA flux and concentration, the model was used to reveal the temporal and spatial
508 distribution of DNA in the lysimeter (Figure 3), which would be difficult to experimentally
509 determine. After injection, the DNA tracer kept moving downward (Figures a1, b1 and c1), and
510 started to move toward the outlet after reaching the variably saturated zone (Figures a2, b2, c2
511 and S1a, S4). However, after reaching the outlet, the spatial distribution of the DNA
512 concentration in the lysimeter showed different transport patterns during day and night time
513 (Figures a2-a7), which agreed with the DNA breakthrough curve (Figure 2d). When there was
514 rainfall input during day time (every day from 8:00 to 18:00), the discharge was increasing in
515 response (Figure 1a), and the DNA tracers moved downward (e.g., from Figure a3 to a4).
516 However, when there was no rainfall input during night (from every day 18:00 to next day 8:00),
517 the discharge started to decrease after reaching the peak at 18:00 (Figure 1a). The drying front,
518 consisting of solid-water-air contact lines, kept moving downward dislodging DNA strands
519 attached to solid surface adsorption sites along their way (e.g., from Figure b4 to b5). As a result,
520 at many locations in the system, the liquid-phase DNA tracer concentration increased, and it

looked like DNA moved upward in the spatial distribution plots during night (e.g., from Figure a4 to a5). On the next day during day time (from 8:00 to 18:00), the cleaned solid surface adsorption sites were available for DNA strands when the wetting front, consisting of solid-water-air contact lines of the reversed direction, passing the solid surface (e.g., from Figure c5 to c6); the new incoming water also diluted the soil pore water. As a result, at many locations in the system, the liquid-phase DNA tracer concentration decreased, and DNA moved downward again in the spatial distribution plots (e.g., from Figure a5 to a6). This diurnal cycle was repeated until the end of the experiment (from Figure a2 to a8). It is clear from the spatial and temporal distribution of attached DNA that the kinetic sorption site 1 was reversible, as the attachment decreased (from Figure b3 to b8) after reached a peak (Figure b3); whereas the kinetic sorption site 2 was irreversible, as the attachment kept increasing (from Figure c1 to c8). Also, except for the initial stage (Figures b1 and c1), the attachment to the kinetic sorption site 1 was one to three magnitude less than the attachment to the kinetic sorption site 2 (comparing Figures b2-b8 to Figures c2-c8). Therefore, the retention of the DNA was dominated by the irreversible kinetic sorption site 2. And this explained why extending the simulation up to 50 days could not improve recovery rate much (Figure S7). More snapshots of DNA concentration, total attached DNA, and DNA attached to the two kinetic sorption sites are available in Figures S8-S11 in the Supporting Information.

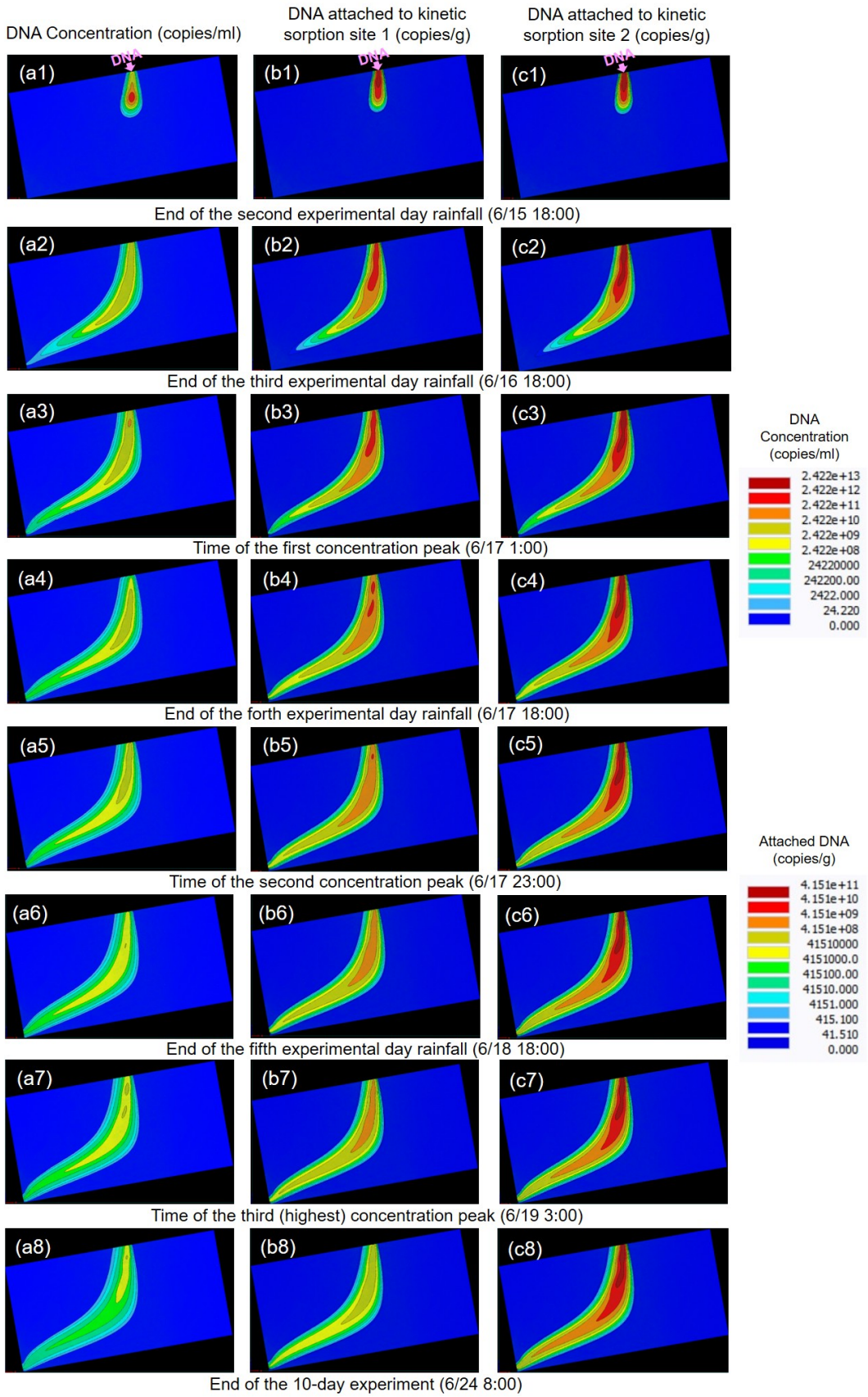
DNA Concentration (copies/ml)
DNA attached to kinetic sorption site 1 (copies/g)
DNA attached to kinetic sorption site 2 (copies/g)
(a1)
(b1)
(c1)
DNA
End of the second experimental day rainfall (6/15 18:00)
(a2)
(b2)
(c2)
End of the third experimental day rainfall (6/16 18:00)
(a3)
(b3)
(c3)
Time of the first concentration peak (6/17 1:00)
(a4)
(b4)
(c4)
End of the forth experimental day rainfall (6/17 18:00)
(a5)
(b5)
(c5)
Time of the second concentration peak (6/17 23:00)
(a6)
(b6)
(c6)
End of the fifth experimental day rainfall (6/18 18:00)
(a7)
(b7)
(c7)
Time of the third (highest) concentration peak (6/19 3:00)
(a8)
(b8)
(c8)
End of the 10-day experiment (6/24 8:00)
DNA Concentration (copies/ml)
2.422e+13
2.422e+12
2.422e+11
2.422e+10
2.422e+09
2.422e+08
24220000
242200.00
2422.000
24.220
0.000
Attached DNA (copies/g)
4.151e+11
4.151e+10
4.151e+09
4.151e+08
41510000
4151000.0
415100.00
41510.000
4151.000
415.100
41.510
0.000

541 **Figure 3.**

Simulated spatial distribution of the DNA tracer in the lysimeter: column (a) is DNA concentration in water, column (b) is DNA attached to the kinetic sorption site 1, and column (c) is DNA attached to the kinetic sorption site 2. Note that the legend of the column (a) is copies of DNA per milliliter of water; while the legend of the columns (b) and (c) is copies of DNA per gram of loamy sand. The selected times were either corresponding to the concentration peaks or were important stages of the experiment.

4. Conclusions

As highlighted by the numerous field and laboratory studies conducted in the past 10 years, synthetic DNA tracers have the potential to realistically mimic microbial and solute tracer (e.g. dyes, bromide, chloride) transport in saturated and unsaturated porous media systems while requiring lower detection limits and lower tracer mass. Yet, many of these studies have purely focused on comparing the transport of synthetic DNA to other conservative tracers in fast-flow systems or in porous media under saturated steady-state conditions.

- In the present work, we have for the first time simulated the transport mechanisms of free synthetic DNA tracers through the vadose zone under variably saturated transient flow condition using the Richards' equation and the Schijven and Šimůnek two-site kinetic sorption model recommended for virus transport modeling in HYDRUS-2D.
- The degradation of the DNA tracer was very slow (estimated to be 10% in 10 days), because the "loamy sand" porous media in our lysimeter was freshly crushed basaltic tephra (i.e.,

562 crushed rocks) and the microbes and DNase that could potentially degrade DNA in regular
563 soils were rare in our “loamy sand”.

564 - The timing of the concentration peaks and the HYDRUS-2D simulated temporal and spatial
565 distribution of DNA in the lysimeter both revealed the role of the solid-water-air contact
566 lines in mobilizing and carrying DNA under the experimental variably saturated transient
567 flow condition. The free DNA was nearly non-selectively transported through the porous
568 media, and showed a slightly early breakthrough, possibly due to a slight effect of anion
569 exclusion or size exclusion.
570 - Overall, the observed and modeled DNA transport presented here suggests that the synthetic
571 DNA tracer share similar transport properties as viruses, as the transport could be captured
572 well by the two-site kinetic sorption model recommended for virus transport modeling.
573 - Given its transport dynamics, synthetic DNA tracers have the potential to be used to trace
574 the transport of viruses and other biocolloids in soil-water systems.
575 - Conducting controlled experiments comparing transport of synthetic DNA tracers and
576 viruses of interest through vadose zone systems and simulating their transport using the two-
577 site kinetic sorption model could improve understanding of the use of synthetic DNA tracers
578 as tracer surrogates to study virus transport in soil-water systems.
579 - The use of synthetic DNA tracers would allow identifying sources and pathways of viruses
580 in the watershed to devise targeted measures to regulate viral source areas such as septic
581 systems or sewage sludge disposal areas within a watershed.

582

Supporting Information

Experimental details, water flow modeling, deuterium tracer transport modeling, inverse modeling details, water flow and hydraulic information, sensitivity analysis, the simulated fate and transport of DNA tracer in the lysimeter.

Notes

The authors declare no competing financial interest.

Acknowledgements

This work was supported by the National Natural Science Foundation of China (grant numbers: 51909264, 52130902); the Heising-Simons Foundation (grant #2014-59); an Axel Wenner-Grens Stiftelse sabbatsstipendium and the Baltic Sea Center and Baltic Nest Institute at Stockholm University. The authors would like to thank Ciaran Harman, Aditi Sengupta, Nathan Abramson, Antônio Meira, Yadi Wang, and the STAR students for their support and help at Biosphere2. And the authors would like to thank the anonymous reviewers' valuable comments helping us improve the modeling and the manuscript.

Author Contributions

The manuscript was written with contributions of all authors. All authors have given approval to the final version of the manuscript.

References

Abbasi, F., Simunek, J., Feyen, J., van Genuchten, M.T., Shouse, P.J., 2003. Simultaneous inverse estimation of soil hydraulic and solute transport parameters from transient field experiments: Homogeneous soil. Transactions of the ASAE, 46(4): 1085. DOI:https://doi.org/10.13031/2013.13960

Aquilanti, L., Clementi, F., Landolfo, S., Nanni, T., Palpacelli, S., Tazioli, A., 2013. A DNA tracer used in column tests for hydrogeology applications. Environmental Earth Sciences, 70(7): 3143-3154.

Attinti, R., Wei, J., Kniel, K., Sims, J.T., Jin, Y., 2010. Virus' (MS2, ϕX174, and Aichi) Attachment on Sand Measured by Atomic Force Microscopy and Their Transport through Sand Columns. Environmental Science & Technology, 44(7): 2426-2432. DOI:10.1021/es903221p

Bear, J., 1972. Dynamics of Fluid in Porous Media. Elsevier, New York.

Carey, G.R., McBean, E.A., Feenstra, S., 2018. Estimating transverse dispersivity based on hydraulic conductivity. Environmental Technology & Innovation, 10: 36-45. DOI:10.1016/j.eti.2018.01.008

Chrysikopoulos, C.V., Katzourakis, V.E., 2015. Colloid particle size-dependent dispersivity. Water Resources Research, 51(6): 4668-4683. DOI:10.1002/2014wr016094

Chu, Y., Jin, Y., Baumann, T., Yates, M.V., 2003. Effect of Soil Properties on Saturated and Unsaturated Virus Transport through Columns. Journal of Environmental Quality, 32(6): 2017-2025. DOI:https://doi.org/10.2134/jeq2003.2017

Chu, Y., Jin, Y., Flury, M., Yates, M.V., 2001. Mechanisms of virus removal during transport in unsaturated porous media. Water Resources Research, 37(2): 253-263. DOI:https://doi.org/10.1029/2000WR900308

627 Clemens, H., Pang, L., Morgan, L.K., Weaver, L., 2020. Attenuation of rotavirus, MS2
628 bacteriophage and biomolecule-modified silica nanoparticles in undisturbed silt loam over
629 gravels dosed with onsite wastewater. Water Research, 169: 115272.
630 DOI:10.1016/j.watres.2019.115272

631 Crist, J.T., McCarthy, J.F., Zevi, Y., Baveye, P., Throop, J.A., Steenhuis, T.S., 2004. Pore-scale
632 visualization of colloid transport and retention in partly saturated porous media. Vadose Zone
633 Journal, 3(2): 444-450.

634 Cupola, F., Tanda, M.G., Zanini, A., 2015. Laboratory estimation of dispersivity coefficients. In:
635 Guadagnini, A., SanchezVila, X., Brunone, B., Ferrante, M., Meniconi, S. (Eds.), 7th
636 Groundwater Symposium of the International Association for Hydro-Environment Engineering
637 and Research. Procedia Environmental Sciences, pp. 74-81. DOI:10.1016/j.proenv.2015.04.011

638 Dahal, U., Adhikari, N.P., 2012. Molecular dynamics study of diffusion of heavy water in normal
639 water at different temperatures. Journal of Molecular Liquids, 167: 34-39.
640 DOI:https://doi.org/10.1016/j.molliq.2011.12.008

641 Dahlke, H.E., Williamson, A.G., Georgakakos, C., Leung, S., Sharma, A.N., Lyon, S.W., Walter,
642 M.T., 2015. Using concurrent DNA tracer injections to infer glacial flow pathways. Hydrological
643 Processes, 29(25): 5257-5274.

644 Gao, B., Saiers, J.E., Ryan, J., 2006. Pore-scale mechanisms of colloid deposition and
645 mobilization during steady and transient flow through unsaturated granular media. Water
646 Resources Research, 42(1). DOI:10.1029/2005wr004233

647 Hassanizadeh, S.M., Schijven, J.F., 2000. Use of bacteriophages as tracers for the study of
648 removal of viruses, IAHS Publ., Liège, Belgium, pp. 167-174.

649 Jin, Y., Chu, Y., Li, Y., 2000. Virus removal and transport in saturated and unsaturated sand
650 columns. Journal of Contaminant Hydrology, 43(2): 111-128.
651 DOI:https://doi.org/10.1016/S0169-7722(00)00084-X

Jin, Y., Flury, M., 2002. Fate and Transport of Viruses in Porous Media. In: Sparks, D.L. (Ed.), Advances in Agronomy. Academic Press, pp. 39-102. DOI:https://doi.org/10.1016/S0065-2113(02)77013-2

Jin, Y., Yates, M.V., Thompson, S.S., Jury, W.A., 1997. Sorption of Viruses during Flow through Saturated Sand Columns. Environmental Science & Technology, 31(2): 548-555. DOI:10.1021/es9604323

Leibundgut, C., Maloszewski, P., Külls, C., 2011. Tracers in hydrology. John Wiley & Sons.

Liao, R., Yang, P., Wu, W., Luo, D., Yang, D., 2018. A DNA Tracer System for Hydrological Environment Investigations. Environmental Science & Technology, 52(4): 1695-1703. DOI:10.1021/acs.est.7b02928

Lorenz, M.G., Wackernagel, W., 1987. Adsorption of DNA to sand and variable degradation rates of adsorbed DNA. Applied and Environmental Microbiology, 53(12): 2948-2952. DOI:10.1128/aem.53.12.2948-2952.1987

Mahmoodlu, M.G., Raoof, A., Bultreys, T., Van Stappen, J., Cnudde, V., 2020. Large-scale pore network and continuum simulations of solute longitudinal dispersivity of a saturated sand column. Advances in Water Resources, 144. DOI:10.1016/j.advwatres.2020.103713

Mandelkern, M., Elias, J.G., Eden, D., Crothers, D.M., 1981. The dimensions of DNA in solution. Journal of Molecular Biology, 152(1): 153-161.

McNew, C.P., Wang, C., Walter, M.T., Dahlke, H.E., 2018. Fabrication, detection, and analysis of DNA-labeled PLGA particles for environmental transport studies. Journal of Colloid and Interface Science, 526: 207-219. DOI:https://doi.org/10.1016/j.jcis.2018.04.059

Meng, W., Xia, Y., Chen, Y., Pu, X., 2018. Measuring the mutual diffusion coefficient of heavy water in normal water using a double liquid-core cylindrical lens. Scientific Reports, 8(1): 12610. DOI:10.1038/s41598-018-30650-z

Mikutis, G., Deuber, C.A., Schmid, L., Kittila, A., Lobsiger, N., Puddu, M., Asgeirsson, D.O., Grass, R.N., Saar, M.O., Stark, W.J., 2018. Silica-Encapsulated DNA-Based Tracers for Aquifer Characterization. Environmental Science & Technology, 52(21): 12142-12152. DOI:10.1021/acs.est.8b03285

Mikutis, G., Schmid, L., Stark, W.J., Grass, R.N., 2019. Length-dependent DNA degradation kinetic model: Decay compensation in DNA tracer concentration measurements. Aiche Journal, 65(1): 40-48. DOI:10.1002/aic.16433

Mortensen, A.P., Hopmans, J.W., Mori, Y., Šimůnek, J., 2006. Multi-functional heat pulse probe measurements of coupled vadose zone flow and transport. Advances in water resources, 29(2): 250-267.

Mualem, Y., 1976. A new model for predicting the hydraulic conductivity of unsaturated porous media. Water Resources Research, 12(3): 513-522.

Nkodo, A.E., Garnier, J.M., Tinland, B., Ren, H., Desruisseaux, C., McCormick, L.C., Drouin, G., Slater, G.W., 2001. Diffusion coefficient of DNA molecules during free solution electrophoresis. Electrophoresis, 22(12): 2424-2432. DOI:10.1002/1522-2683(200107)22:12<2424::AID-ELPS2424>3.0.CO;2-1

Pang, L., Abeysekera, G., Hanning, K., Premaratne, A., Robson, B., Abraham, P., Sutton, R., Hanson, C., Hadfield, J., Heiligenthal, L., Stone, D., McBeth, K., Billington, C., 2020. Water tracking in surface water, groundwater and soils using free and alginate-chitosan encapsulated synthetic DNA tracers. Water Research, 184: 116192. DOI:https://doi.org/10.1016/j.watres.2020.116192

Pang, L.P., Farkas, K., Bennett, G., Varsani, A., Easingwood, R., Tilley, R., Nowostawska, U., Lin, S.S., 2014. Mimicking filtration and transport of rotavirus and adenovirus in sand media using DNA-labeled, protein-coated silica nanoparticles. Water Research, 62: 167-179. DOI:10.1016/j.watres.2014.05.055

Pangle, L.A., DeLong, S.B., Abramson, N., Adams, J., Barron-Gafford, G.A., Breshears, D.D., Brooks, P.D., Chorover, J., Dietrich, W.E., Dontsova, K., 2015. The Landscape Evolution Observatory: A large-scale controllable infrastructure to study coupled Earth-surface processes. Geomorphology, 244: 190-203.

Powelson, D.K., Mills, A.L., 2001. Transport of Escherichia coli in sand columns with constant and changing water contents. Journal of Environmental Quality, 30(1): 238-245.

Ptak, T., Piepenbrink, M., Martac, E., 2004. Tracer tests for the investigation of heterogeneous porous media and stochastic modelling of flow and transport—A review of some recent developments. Journal of Hydrology, 294(1-3): 122-163.

Raoof, A., Hassanizadeh, S.M., 2013. Saturation-dependent solute dispersivity in porous media: Pore-scale processes. Water Resources Research, 49(4): 1943-1951. DOI:10.1002/wrcr.20152

Romanowski, G., Lorenz, M.G., Wackernagel, W., 1993. Plasmid DNA in a groundwater aquifer microcosm -adsorption, DNAase resistance and natural genetic transformation of Bacillus subtilis. Molecular Ecology, 2(3): 171-181. DOI:https://doi.org/10.1111/j.1365-294X.1993.tb00106.x

Sabir, I.H., Torgersen, J., Haldorsen, S., Aleström, P., 1999. DNA tracers with information capacity and high detection sensitivity tested in groundwater studies. Hydrogeology Journal, 7(3): 264-272.

Schijven, J.F., Šimůnek, J., 2002. Kinetic modeling of virus transport at the field scale. Journal of Contaminant Hydrology, 55(1): 113-135.

Sengupta, A., Wang, Y., Neto, A.A.M., Matos, K.A., Dontsova, K., Root, R., Neilson, J.W., Maier, R.M., Chorover, J., Troch, P.A., 2016. Soil Lysimeter Excavation for Coupled Hydrological, Geochemical, and Microbiological Investigations. JoVE(115): e54536-e54536.

Sharma, A.N., Luo, D., Walter, M.T., 2012. Hydrological tracers using nanobiotechnology: Proof of concept. Environmental Science & Technology, 46(16): 8928-8936.

Šimůnek, J., Jacques, D., Langergraber, G., Bradford, S.A., Šejna, M., van Genuchten, M.T., 2013. Numerical modeling of contaminant transport using HYDRUS and its specialized modules. Journal of the Indian Institute of Science, 93(2): 265-284.

Šimůnek, J., van Genuchten, M.T., Gribb, M.M., Hopmans, J.W., 1998. Parameter estimation of unsaturated soil hydraulic properties from transient flow processes. Soil and Tillage Research, 47(1): 27-36. DOI:https://doi.org/10.1016/S0167-1987(98)00069-5

Šimůnek, J., van Genuchten, M.T., Sejna, M., 2008. Development and applications of the HYDRUS and STANMOD software packages and related codes. Vadose Zone Journal, 7(2): 587-600.

Šimůnek, J., van Genuchten, M.T., Šejna, M., 2016. Recent developments and applications of the HYDRUS computer software packages. Vadose Zone Journal, 15(7).

Sirois, S.H., Buckley, D.H., 2019. Factors governing extracellular DNA degradation dynamics in soil. Environmental Microbiology Reports, 11(2): 173-184. DOI:10.1111/1758-2229.12725

Stumpp, C., Stichler, W., Kandolf, M., Simunek, J., 2012. Effects of land cover and fertilization method on water flow and solute transport in five lysimeters: A long-term study using stable water isotopes. Vadose Zone Journal, 11(1): n/a. DOI:10.2136/vzj2011.0075

van Genuchten, M.T., 1980. A closed-form equation for predicting the hydraulic conductivity of unsaturated soils. Soil Science Society of America Journal, 44(5): 892-898.

Wang, C., McNew, C.P., Lyon, S.W., Walter, M.T., Volkman, T.H.M., Abramson, N., Sengupta, A., Wang, Y., Meira Neto, A.A., Pangle, L., Troch, P.A., Kim, M., Harman, C., Dahlke, H.E., 2019. Particle tracer transport in a sloping soil lysimeter under periodic, steady state conditions. Journal of Hydrology, 569: 61-76. DOI:https://doi.org/10.1016/j.jhydrol.2018.11.050

Wang, C., Wang, R., Huo, Z., Xie, E., Dahlke, H.E., 2020. Colloid transport through soil and other porous media under transient flow conditions—A review. WIREs Water, 7(4): e1439. DOI:10.1002/wat2.1439

Xue, J., Feng, Y., 2018. Determination of adsorption and desorption of DNA molecules on freshwater and marine sediments. Journal of Applied Microbiology, 124(6): 1480-1492. DOI:10.1111/jam.13739

Zhang, Y.R., Hartung, M.B., Hawkins, A.J., Dekas, A.E., Li, K.W., Horne, R.N., 2021. DNA Tracer Transport Through Porous Media-The Effect of DNA Length and Adsorption. Water Resources Research, 57(2). DOI:10.1029/2020wr028382